Investigation of Laser Processing of Biodegradable Nanofiber Nonwovens with Different Laser Pulse Durations

M. Götze[1], T. Kürbitz[2,3], O. Krimig[1], C.E.H. Schmelzer[3], A. Heilmann[2,3] and G. Hillrichs[1]

[1] *University of Applied Sciences Merseburg, Eberhard-Leibnitz-Str.2, 06217 Merseburg, Germany*
E-mail: marco.goetze@hs-merseburg.de
[2] *University of Applied Sciences Anhalt, Bernburger Str. 55, 06266 Köthen, Germany*
[3] *Fraunhofer Institute for Microstructure of Materials and Systems IMWS, Walter-Hülse-Str.1, 06120 Halle (Saale), Germany*

Implants or cell carriers made of biopolymers or biodegradable polymers are well suited for the regeneration of defects in various tissues. They act as an adhesion surface for autologous cells and provide sufficient stability. Electrospun nonwovens have a favourable surface to volume ratio and mimic the structure of the fiber proteins of the extracellular matrix in tissues. Their high porosity ensures a sufficient supply of nutrients to the cells while maintaining high mechanical strength. In addition, drug-release functionality can be installed in biodegradable nonwovens, which can support the regeneration. Particularly promising are flakes made of electrospun nonwovens which, in an appropriate suspension, can be injected into defective areas. For the production of such flakes, laser cutting or surface structuring can be applied. Typically, ablation by ultrashort laser pulses reduces the heat-affected zones significantly in microprocessing of many polymers. In this work, the quality of processing of electrospun gelatine and poly-lactide (PLA) nonwovens was investigated for UV-solid-state lasers with pulse durations in the nano- and picosecond range. We observed comparable ablation quality of electrospun gelatine nonwovens with UV nanosecond and with UV picosecond ablation. A similar behaviour was found for electrospun PLA nonwovens. Higher pulse energy was necessary for nanosecond ablation with the same focal spot diameter.

DOI: 10.2961/jlmn.2019.01.0012
Keywords: picosecond laser, laser ablation, nanosecond laser, polylactide nanofibers, gelatine nanofibers, nanofiber scaffold, electrospinning

1. Introduction

Nonwovens (NW) made from electrospun polymers are currently part of many research activities, especially in the field of regenerative medicine [1–4]. The reason for this is the possibility to produce nonwovens with high porosity and fiber diameters in the micrometer and nanometer range with the electrospinning process for a large number of polymers. Especially for the development of processes for tissue regeneration, there is great potential due to the similarity of the generated structures to the protein fiber network in the extracellular matrix (ECM). Also, the use of biodegradable polymers such as poly-lactic acid (PLA), polylactic-co-glycolic acid (PLGA), polycaprolactone (PCL) or biopolymers such as collagen and gelatine were investigated intensively [5–9]. However, the good porosity of the nonwovens, resulting in a good surface-to-volume ratio and good nutrient supply to attached cells, is accompanied by an often too small pore size to promote growth of the cells in or through the nonwovens. Due to their precise and contactless processing, laser-based methods offer a good opportunity to create voids in the nanofiber network to improve cell proliferation [10,11]. Also the generation of injectable flakes in the submillimeter range is a field for laser processing. Thus lasers were used to create holes in nonwovens made of PCL, gelatine and PLGA to replace damaged tooth tissue, bone tissue and to create corneal implants [12–14]. Different pulsed laser sources with pulse durations from a few µs to fs in the UV, green and IR wavelength range were used. In particular, ultrashort pulsed lasers in the femtosecond range are interesting for such treatments, because they typically ablate material without significant thermal damage and thereby preserve the structure of the nonwovens. Previous investigations on polyamide (PA) nonwovens have shown, that even pulse durations in the picosecond range are sufficient to minimize thermal damage [15]. It was also shown, that pulse durations in the nanosecond range leads to more thermal damage to the PA nonwoven. In the work presented here, laser processing of nanofiber nonwovens of the biodegradable polymer PLA and the biopolymer gelatine was investigated with different laser pulse durations and compared with processing of PLA bulk polymer.

2. Material and methods

2.1 Electrospinning

Via the electrospinning process, it is possible to produce polymer fibers from dissolved polymers in an electric field. Depending on the process parameter, fibers of different lengths and diameters in the nanometer range are possible. In the current work, gelatine (Gelita Imagel HP) was dissolved in 50% acetic acid (Carl Roth) to a concentration of 20% (w/v). The commercial nozzle-free electrospinning device “Nanospider” (Elmarco) was used for the gelatine nonwovens. The process was carried out at 80 kV with a working distance of the electrodes at 240 mm.

PLA was dissolved in HFIP (Alfa Aesar) to a concentration of 10% (w/v) and electrospun on a different "single nozzle" electrospinning device. The working distance of the needle tip and the collecting electrode was 120 mm, with a voltage of 25 kV and a flowrate of 10µl/min. For both materials the fiber size distribution was measured by analysing SEM-Images (Fig. 1 and 2). The fiber diameter of the PLA-fibers are in the micrometer range and bigger than for the gelatine fibers.

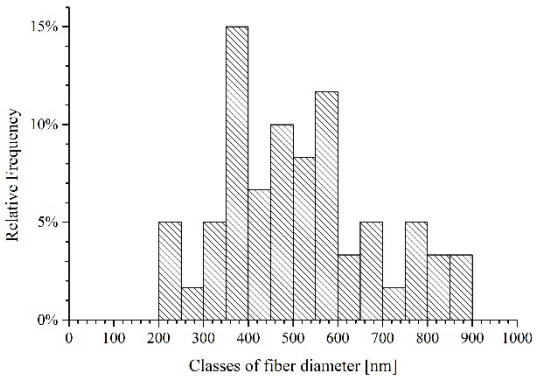

Fig. 1 Fiber diameter distribution of PLA nonwovens.

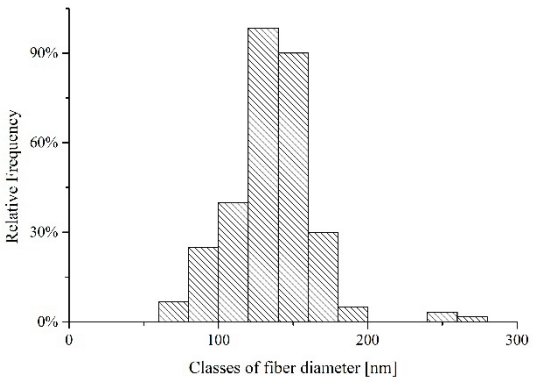

Fig. 2 Fiber diameter distribution of gelatine nonwovens.

To estimate the density ρ_{nw} of the nonwovens, samples with 2 cm x 2 cm areas were balanced. The thickness of the samples (about 130 µm for PLA-NW and 120 µm for gelatine-NW) was measured by confocal microscopy. It was found that ρ_{nw} is about 0.1 g/cm³ for gelatine-nonwovens and 0,18 g/cm³ for PLA-nonwovens. For bulk PLA a bulk density ρ_B of 1.25 g/cm³ and for gelatine 1.35 g/cm³ was determined. The porosity p_{nw} [16] of the nonwovens was calculated by $p_{nw}=(\rho_B - \rho_{nw})/\rho_B$ and found to be about 84 % for both materials. For comparison poly-L-lactic acid bulk material (Goodfellow) with a thickness of 50µm was used.

2.2 Laser Systems

A picosecond laser from Coherent (Talisker, Table 1) and a nanosecond laser from Coherent (Matrix 355, Table 2) were used. Both lasers were integrated in the same laser micromachining workstation. A galvoscanning system (Nutfield) guided the laser beam across the sample. The sample could also be moved using a computer-controlled x-y-z stage. The beam is focused by f-theta lenses (f = 103 mm). The measured Spot sizes for both lasers is about 14 µm.

Table 1 Data of the picosecond laser

Picosecond laser (Coherent Talisker)	
Wavelength	355 nm
Pulse duration	15 ps
Max. pulse energy	20 µJ
Max. pulse repetition rate	up to 200 kHz
Beam quality M^2	<1.3
Focal spot diameter	14 µm
Focusing angle (full)	~3.1°

Table 2 Data of the nanosecond laser

Nanosecond laser (Coherent Matrix 355)	
Wavelength	355 nm
Pulse duration	30 ns
Max. pulse energy	88 µJ
Pulse repetition rate	50 kHz
Beam quality M^2	<1.3
Focal spot diameter	14 µm
Focusing angle	~3.1°

2.3 Experimental Setup

For processing of nanofibers nonwovens, they were clamped "free hanging" in a sample holder so that for cutting and drilling there is no interaction of the laser beam with a nearby supporting structure.

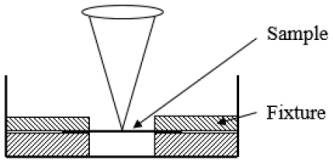

Fig. 3 Sample holder for "free hanging" processing

The laser processed structures are evaluated by optical microscopy (Olympus BX50), confocal optical microscopy (OPM Messtechnik KFM) and scanning electron microscopy (LOT Phenom, Tescan Vega 3).

3. Results and discussion

3.1 Ablation thresholds

The ablation threshold F_{th} is the minimum laser fluence, at which a significant material removal can be observed [17]. To determine the single pulse threshold fluence $F_{th}^{N=1}$, material was removed on the examined materials in the focal

plane of the focusing lens by single-pulse ablation. By varying the laser fluence, different sized holes were generated (Fig. 4).

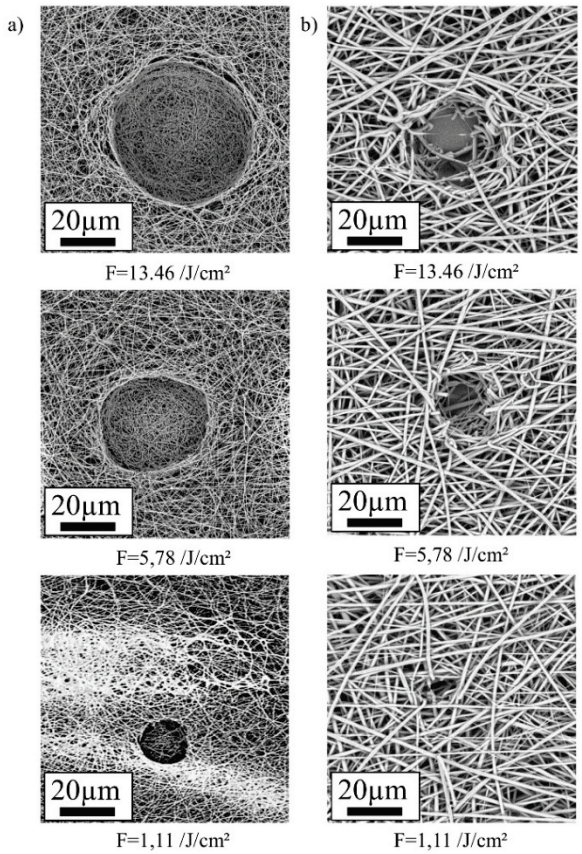

Fig. 4 Single pulse structures created with picosecond laser irradiation on a) electrospun gelatine nonwovens and b) electrospun-PLA-nonwovens with different laser fluences used.

The structure diameters were measured in the SEM images. The relation between D^2 and pulse energy Q is given by [18,19]

$$D^2(Q) = 2w^2 \cdot ln\left(\frac{Q}{Q_{th}}\right) \quad (1)$$

From the slope of D^2 as a function of ln(Q), the effective radius of the beam on the surface w can be obtained. For bulk materials w corresponds to the Gaussian radius of the beam on the surface. For the highly porous nonwovens the effective area of interaction of the laser beam with the sample is increased by light scattering [20,21]. The relation between D^2 and the applied laser fluence F_0^{av} is given by [18,19]

$$D^2(F_0^{av}) = 2w^2 \cdot ln\left(\frac{F_0^{av}}{F_{th}}\right) \quad (2)$$

The fluences are calculated with the beam radii w given in Table 3. From the slope and from the fluence axis intercept of linear fits to the measured data $D^2(\ln(F_0^{av}))$, ablation threshold F_{th} can be calculated.

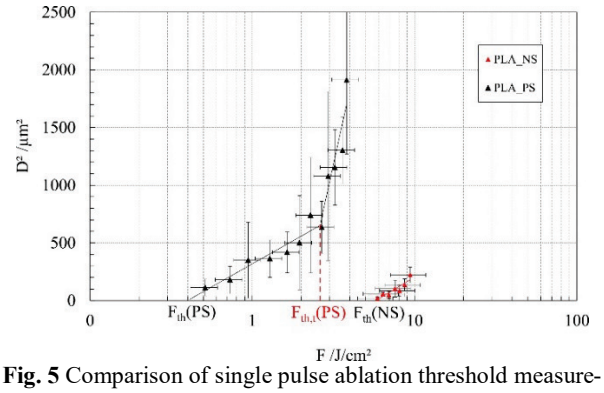

Fig. 5 Comparison of single pulse ablation threshold measurements of PLA-nonwovens processed with ps- and ns-laser pulses.

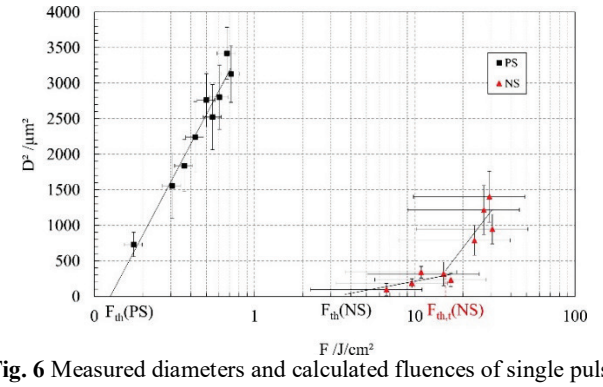

Fig. 6 Measured diameters and calculated fluences of single pulse ablation spots created with ps- and ns-laser pulses on gelatine nonwovens. The intercepts of the linear fits with the x-axis indicates the ablation thresholds F_{th}.

For some materials, it is possible that, above a certain thermal threshold fluence $F_{th,t} > F_{th}$, the diameter of the ablated structure is significantly larger than expected from Eq.2. Gevilas et al. and Engelhardt et al. explained this behaviour with photochemical- and photothermal dominated ablation in different fluence ranges. In the fluence range between F_{th} and $F_{th,t}$ ablation by direct breaking of chemical bonds by single- or multiphoton absorption dominates. Above the thermal threshold the laser pulse deposits more energy into the material than needed for the ablation process and induces melting [22,23]. Also optical radiation due to plasma formation could increase the thermal influence and thus the structure size [21]. The results of the single-pulse threshold fluence measurements are summarized in Table 3. Where $F_{th,t}$ has been determined, these are also listed.

The threshold fluences decrease with the pulse duration. For the nonwoven materials, the single pulse thresholds for ps-processing with 0.39 J/cm² (PLA) and 0.126 J/cm² (gelatine) are smaller than the thresholds for ns-processing with 5.78 J/cm² (PLA) and 3.13 J/cm² (gelatine). Probably, the smaller thermal stability of gelatine promotes removal of material. For comparison, for polyamide nonwovens with similar fiber diameters and a better thermal stability, a threshold fluence of 0.12 J/cm² was found (355nm, 15ps [15]), which is close to the gelatine-NW threshold. This suggests that the fiber diameters have a decisive influence on F_{th}.

The influence of porosity on the threshold fluence becomes particularly clear when comparing the results of the NW with the bulk material. The threshold fluence of PLA bulk material is significantly higher with 1.4 J/cm² (ps) and 27 J/cm² (ns).

Table 3 Single pulse ablation thresholds (fluence and intensity), thermal thresholds (fluence) and calculated beam radius w for 355 nm lasers (pulse duration 30 ns and 15 ps).

Materials	F_{th} /J/cm²	I_{th} /(10^{10}W/cm²)	$F_{th,t}$ /J/cm²	w /µm
PLA-NW - 15 ps	0.39	2.6	3	13.1
PLA-NW - 30 ns	5.78	0.019	-	13.6
PLA-Bulk - 15 ps	1.4	9.3	-	4.4
PLA-Bulk - 30ns	6.8	0,023	-	6.4
Gelatine-NW - 15ps	0.126	7.5	3	30.4
Gelatine-NW - 30ns	3.13	0.010	20	9.6

By determining multipulse ablation thresholds, it is possible to draw further conclusions on the removal behaviour of materials. For this purpose, the ablation spot diameters were measured as a function of the pulse number and evaluated according to the D² model for ps- and ns-processing of PLA-bulk material. For the nonwoven materials, this was not possible because they are too thin. Fig. 7 shows the single and multipulse thresholds for 1, 10 and 100 pulses. The linear fit of the threshold fluences characterizes the incubation factor ξ [24], which was calculated with

$$F_{th}(N) = F_{th}(N=1)N^{\xi-1} \quad (3)$$

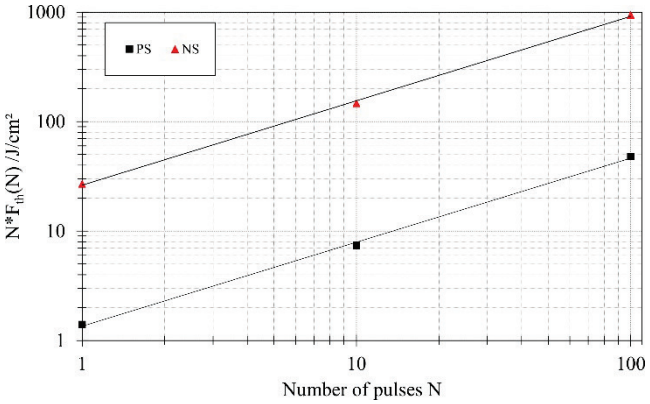

Fig. 7 Ablation thresholds for single- and multipulse ablation (10 and 100 pulses) for ps- and ns-processing of PLA-Bulk material. The linear fit describes the incubation behavior of the material and thus the incubation factor ξ.

The incubation factor ξ describes the incubation behavior of materials when processed with multiple pulses. Incubation occurs when previous laser pulses cause pre-damage in the material, e.g. structural changes below the ablation threshold, a loosening in the polymer chains by bond breaks or by heating of the material, which does not immediately lead to a material removal. These pre-damages facilitate the material removal by subsequent pulses, So, less energy is needed and the ablation threshold decreases. With ξ = 1 no incubation effect occurs. For PLA bulk material, a ξ of 0.77 was determined for both ps- and ns-machining (Fig.7). This means, that slight incubation occurs. This is comparable to other materials such as polycarbonate (0.74) and PA-NW (0.78) and smaller than PA bulk (0.64) [25].

Another approach for determining the ablation thresholds is the logarithmic dependence of the ablation depth h to the fluence F_0^{av} described in [19,23,26] (Fig. 8):

$$h = \alpha_{eff}^{-1}\left(\frac{F_0^{av}}{F_{th}}\right) \quad (4)$$

where α_{eff}^{-1} is the optical penetration depth of the material.

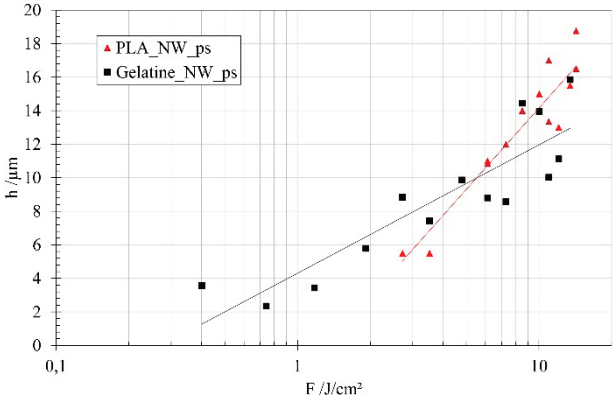

Fig. 8 Measured ablation depths for ps-ablation of PLA- and gelatin NW at different laser fluences.

The slope of the linear fit to the data h(ln(F_0^{av})) gives the optical penetration depth α_{eff}^{-1}, which is 5.7µm (PLA-NW) and 3.32µm (gelatine-NW) for ps-processing. For nanosecond processing of gelatine-NW, a higher penetration depth of about 60 µm was determined.

3.2 Process Quality/ Cutting quality

In addition to the ablation threshold measurements, cutting tests were performed. This is especially interesting with regard to the production of submillimeter injectable flake suspensions of the nonwovens. To maintain the positive properties of the nonwovens, the heat affected zone (HAZ) should be as small as possible. Especially for gelatine-nonwovens, excessive thermal influence causes carbonization, which can possibly trigger cytotoxic or inflammatory reactions in the body. For these experiments, the pulse overlap and the laser fluence were varied and the samples were evaluated by means of SEM images with regard to processing quality and HAZ. For ps-processing, the influence of the temporal pulse spacing was also examined. For the nanosecond laser, this was not possible since the pulse energy and pulse duration change with the repetition rate.

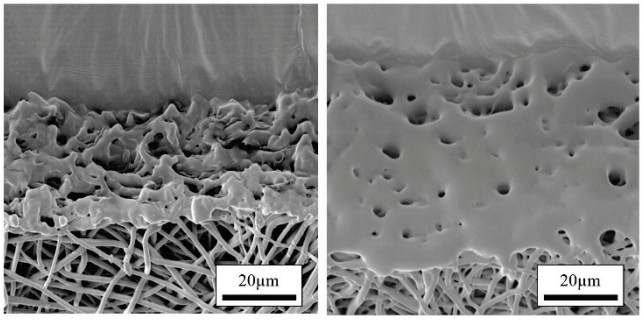

Fig. 9 SEM-images of PLA-NW cutting edges produced with ps-laser irradiation and with spatial pulse distances of about 4µm. The samples were tilted by 45°. Left: v=50mm/s, f=12.5kHz; right: v=800mm/s, f=200kHz.

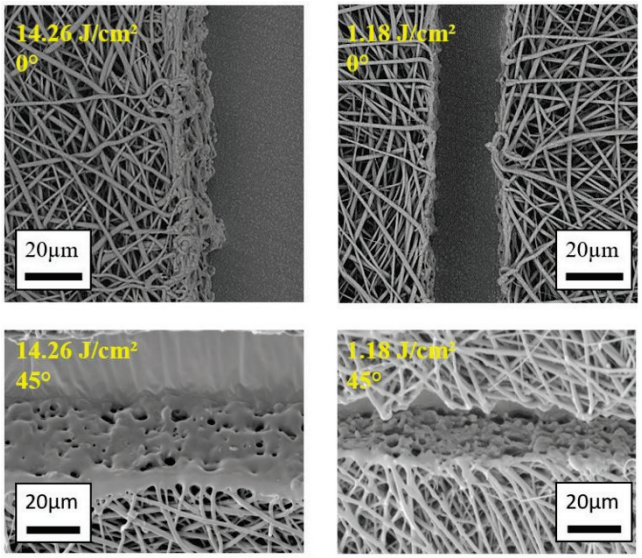

Fig. 10 Cutting edges of PLA-NW processed with τ=15ps, v=50mm/s, f=50kHz and different laser fluences. In the bottom row the samples were tilted by 45°.

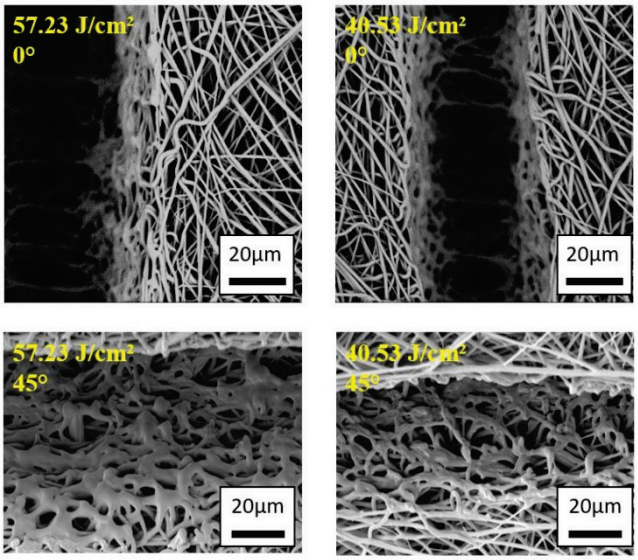

Fig. 11 Cutting edges of PLA-NW processed τ=30ns, v=50mm/s, f=50kHz and different laser fluences. In the bottom row the samples were tilted by 45°.

With both laser sources, the surface of the samples shows only small HAZ of a few micrometers when processing PLA-NW. A slight merging of thinner fibers to thicker fibers and larger melting areas in the region of the cutting edge (Fig. 9 - 11) can be observed. For high fluences (14.26 J/cm² for ps- and 57.23 J/cm² for ns-processing) the walls of the cuts show thin melting films. The films are not completely closed, so that the supply of cells with nutrients is also possible in these regions. A significant reduction of the fluence in ps-processing to 1.18 J/cm² improves the quality of the walls even further. For ns-processing, a good wall quality could be achieved with a fluence of about 40 J/cm² (Fig. 11).

While using the same fluences and spatial pulse distances, the influence of the repetition rate has been evaluated. A significant fusion along the PLA-NW cutting edge was observed in ps-processing with high repetition rates (Fig. 9).

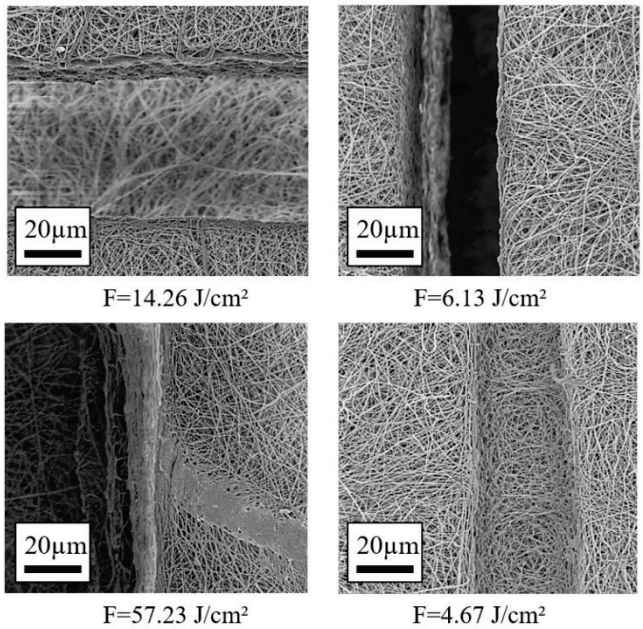

Fig. 12 Cutting edges of gelatine-NW processed with different fluences. Top: τ=15ps, v=50mm/s, f=50kHz; Bottom: τ=30ns, v=50mm/s, f=50kHz

Similar to the processing of the PLA-NW, it is possible to reduce the HAZ of the gelatine-NW to a few microns when using moderate fluences (Fig. 12).

3.3 Ablation Mechanism

Polymer ablation is generally considered to be a photophysical process in which both thermal and non-thermal fractions contribute to ablation [27]. Photochemical ablation is often called “cold ablation” due to the fact that the excitation of the chemical bonds occurs at energy levels above the dissociation energy. This results in direct bond breaking and formation of small, mostly volatile fragments. These numerous fragments require a large volume, so that in the irradiated volume, a high pressure builds up and it comes to an explosive evaporation of the material. Normally, this process is too fast to transfer energy from the fragments to the polymer, so that in the photochemical mechanism the average heating of the material is small [28]. This leads normally to sharp edges. If the photon energy E_P is large enough, linear absorption of the photons can lead to direct bond breaking

in polymers. At a wavelength of $\lambda = 355$nm, the photon energy is $E_P = 3.49$eV. With this photon energy, it is possible to break C-N bonds ($E_B = 3.04$eV) of gelatine [23]. On the other hand, PLA has no C-N bonds, which could be broken through single-photon absorption. Compared with ps ablation, for ns processing smaller multiphoton absorption is expected in the intensity range used here. It is assumed that the ns ablation of PLA is predominantly due to heating, which leads to melting, evaporation and to thermally induced stress in the material. The lack of the possibility to break PLA bonds photochemically may also be the reason that the PLA nonwovens have a higher single pulse ablation threshold for ns processing than gelatine nonwovens (Table 3).

Due to the higher peak intensity at ps pulse durations, it is expected that the absorption of the laser radiation is enhanced by multiphoton absorption. Thus, direct bond breaking and ablation is possible with $E_P < E_B$ [17].

Considering the ratio of the respective single pulse ablation thresholds to the pulse durations used, one obtains $F_{th,ps}/F_{th,ns} = 0.067$ for PLA nonwovens. For one-dimensional heat conduction in the material, it is expected, that the ratio $F_{th,ps}/F_{th,ns} = (\tau_{PS}/\tau_{NS})^{\varepsilon}$ [17]. In the approximation of 3D heat conduction $\varepsilon = 1$, while for purely 1D-heat conduction $\varepsilon=0.5$ is expected. For the pulse durations used here $(\tau_{PS}/\tau_{NS})^{\varepsilon}$ is 0.005 ($\varepsilon=1$) and 0.022 ($\varepsilon=0.5$). So for PLA- nanofibers the ablation is dominated by 1D heat conduction. For gelatine nanofibers, $F_{th,ps}/F_{th,ns} = 0.03$, so that also predominantly 1D-heat conduction can be assumed. This indicates, that the thermal penetration depth into the nanofiber nonwoven samples is smaller than the effective size of the laser spots on the sample surface.

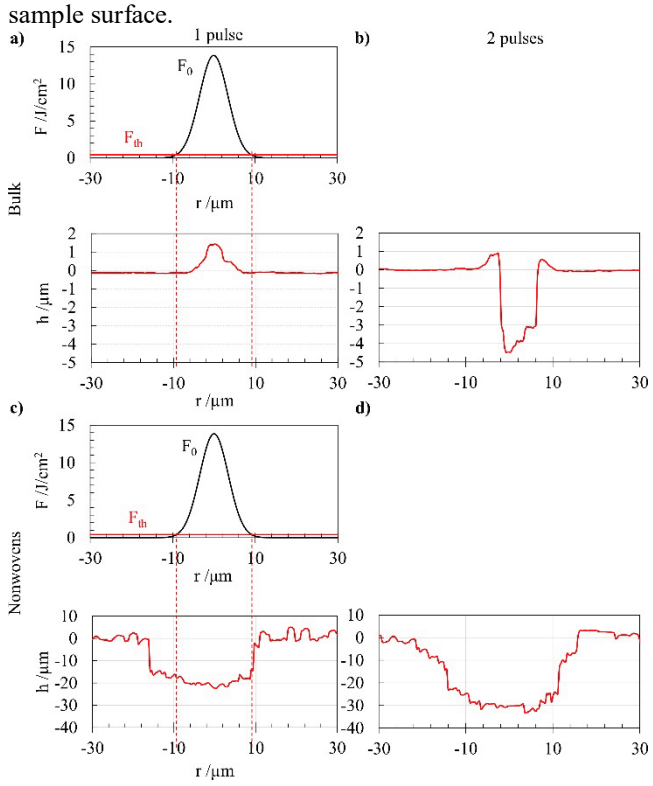

Fig. 13 Surface profiles after ps-processing. a) Comparison of the Gaussian beam profile with the surface structure obtained by a single laser pulse on PLA-bulk material. b) PLA-bulk ablation site after 2 ps-pulses. c) Beam profile with ablation threshold compared to the single pulse structure size of PLA-NW. d) Ablation structure of PLA-NW after 2 ps-pulses.

It was found, that for single-pulse processing of PLA bulk material with the ps-laser, a hump arises on the surface for all available fluences. In Fig. 13a it is shown that the diameter of the hump is in the expected structure size range. The hump formation was neither observed for ps-laser nor for ns-laser processing of nonwovens. Also, the actual feature size is larger for the nonwovens (Fig. 13c). Additional laser pulses on the bulk material lead to hole formation (Fig. 13b). The formation of humps has already been observed in single-pulse PS ablation of PA6.6 [25] and also for nanosecond ablation of PI, PMMA [27] and PLA [29,30]. It was explained by a volume increase by amorphisation of crystalline-domains and trapped polymer fragments in the interaction volume [17]. It can be assumed, that restructuring processes in the near-surface layer of the semicrystalline PLA, as well as the formation of gaseous products, like CO and CO_2, below the surface lead to this humps [30]. The absence of the humps for the nonwoven is probably due to the high porosity. Gaseous molecules formed by the laser interaction can diffuse out of the nonwovens rapidly without changing the volume.

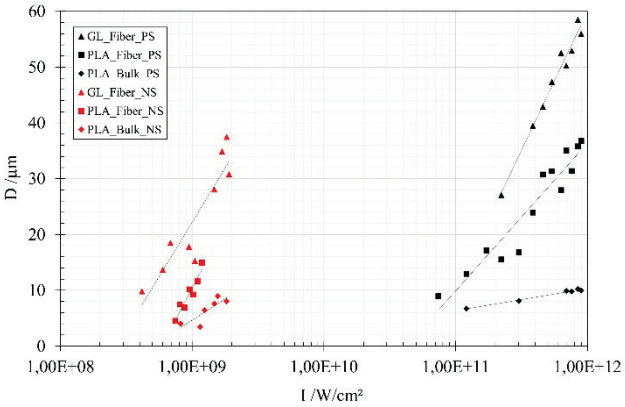

Fig. 14 Fiber diameters of PLA- and gelatine-NW (GL) and PLA-bulk material after ps- and ns-single pulse processing, as a function of laser intensity.

As shown in Fig. 14, for both laser sources, significantly larger ablation structures were measured on the nonwovens than on the bulk material. The measured ablation diameters for gelatine nonwovens are even greater than those for PLA nonwovens. In Fig. 15 and 16 the ablation profiles for ps- and ns-processing of PLA-nonwovens after 3 pulses are shown. Compared with the bulk material, in the nonwovens, the ablations sites are more extended in lateral and the vertical dimensions. One obvious reason for this is the porosity of the nonwovens in contrast to the compact bulk material. Surprisingly, for ns radiation (Fig. 15) the ablated nonwoven volume is smaller than for ps ablation (Fig. 16). Typically, for bulk materials the opposite is expected. Park et al. demonstrated with electrospun PCL nonwovens that the light scattering of fs laser radiation is very large. The irradiated nonwoven volume is stronger determined by scattering than by absorption [20]. Light scattering in the Mie range should not depend on the intensity, while the effective absorption in the fibers is intensity dependent due to nonlinear effects. So the volume penetrated by radiation should be similar for ns- and ps-pulses. Possibly, due to the lower ps ablation threshold a bigger volume is ablated by ps pulses than by ns pulses. However, the interplay between threshold fluence, scattering, absorption, thermal penetration depth

and mechanical and shock wave propagation play a role in a complete description of nonwoven ablation and should be evaluated further.

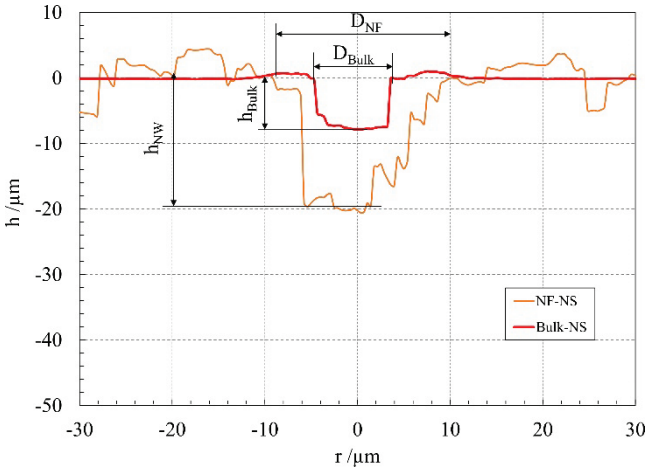

Fig. 15 Ablation profile of PLA-NW and PLA-bulk material after 3 nanosecond pulses.

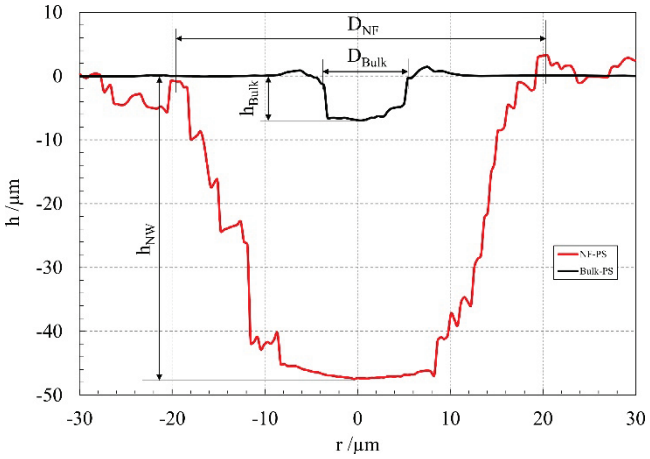

Fig. 16 Ablation profile of PLA-NW and PLA-bulk material after 3 picosecond pulses.

4. Conclusion

For electrospun PLA- and gelatine nonwovens, the single pulse ablation thresholds were determined for ps- and ns-laser pulses at 355 nm. The threshold fluences for ps-processing are smaller than for ns-processing, and smaller for gelatine nonwovens than for PLA nonwovens. The peptide bonds in the gelatine appear to favor processing by UV-NS lasers, leading to smaller ablation thresholds compared with PLA-nonwovens. For PLA bulk material, a slight incubation effect for multi-pulse processing was determined for both ps- and ns-processing. With regard to the cutting quality for the nonwovens, sharp cutting edges with very small heat affected zones could be achieved for both PLA and gelatine nonwovens at moderate fluences. Thus, UV-ns-processing of electrospun PLA and gelatin is a good alternative to UV-ps-processing. Processing of PLA nonwovens with UV-ns-pulses requires larger fluences than processing of gelatine nonwovens.

With the same laser parameters, larger ablation sites were created on the nonwovens than on the bulk material. The fineness of the structures is not limited by the Gaussian beam but strongly determined by other effects such as light scattering in the fiber network. These effect has to be investigated further.

Acknowledgments

This work was carried out within the program "Forschung an Fachhochschulen – Förderlinie Ingenieurnachwuchs ", FKZ: 13FH017IA5 and funded by the Federal Ministry of Education and Research (BMBF). We are grateful to Denis Wiegandt for his support in several experiments and to Arpita Desai for the nanofiber diameter measurements. We also thank Coherent for supporting us with the Matrix laser system.

References

[1] K. Szustakiewicz, B. Stępak, A. J. Antończak, M. Maj, M. Gazińska, B. Kryszak, and J. Pigłowski: Polym. Degrad. Stab., 149, (2018), 152.
[2] Y.-C. Jiang, L. Jiang, A. Huang, X.-F. Wang, Q. Li, and L.-S. Turng: Mater. Sci. Eng., C, 71, (2017), 901.
[3] Q. Yao, J. G.L. Cosme, T. Xu, J. M. Miszuk, P. H.S. Picciani, H. Fong, and H. Sun: Biomaterials, 115, (2017), 115.
[4] J. Idaszek, E. Kijeńska, M. Łojkowski, and W. Swieszkowski: Appl. Surf. Sci., 388, (2016), 762.
[5] A. Daskalova, B. Ostrowska, A. Zhelyazkova, W. Święszkowski, A. Trifonov, H. Declercq, C. Nathala, K. Szlazak, M. Lojkowski, W. Husinsky, and I. Buchvarov: Appl. Phys. A, 124, (2018),
[6] F. Diomede, A. Gugliandolo, P. Cardelli, I. Merciaro, V. Ettorre, T. Traini, R. Bedini, D. Scionti, A. Bramanti, A. Nanci, S. Caputi, A. Fontana, E. Mazzon, and O. Trubiani: Stem Cell Research & Therapy, 9, (2018), 1.
[7] R. Ortiz, S. Moreno-Flores, I. Quintana, M. Vivanco, J. R. Sarasua, and J. L. Toca-Herrera: Mater. Sci. Eng., C, 37, (2014), 241.
[8] A. Shibata, M. Machida, N. Kondo, and M. Terakawa: Appl. Phys. A, 123, (2017), 457.
[9] J. S. Fernandes, P. Gentile, M. Martins, N. M. Neves, C. Miller, A. Crawford, R. A. Pires, P. Hatton, and R. L. Reis: Acta Biomat., 44, (2016), 168.
[10] C.-H. Chen, M.-Y. Lee, V. B.-H. Shyu, Y.-C. Chen, C.-T. Chen, and J.-P. Chen: Mater. Sci. Eng., C, (2014), 389.
[11] B. L.-P. Lee, H. Jeon, A. Wang, Z. Yan, J. Yu, C. Grigoropoulos, and S. Li: Acta Biomat., 8, (2012), 2648.
[12] J. Aragon, N. Navascues, G. Mendoza, and S. Irusta: Int. J. Pharm., 525, (2017), 112.
[13] C. Ma, T. Qu, B. Chang, Y. Jing, J. Q. Feng, and X. Liu: Adv. Healthcare Mater., 7, (2018),
[14] B. Kong, W. Sun, G. Chen, S. Tang, M. Li, Z. Shao, and S. Mi: Sci. Rep., 7, (2017),
[15] M. Götze, A. Mannan Farhan, T. Kürbitz, O. Krimig, S. Henning, A. Heilmann, and G. Hillrichs: J. Laser Micro/Nanoengin., 12, (2017), 286.
[16] Sudhakara Sarma Sreedhara, Narasinga Rao Tata: J. Eng. Fibers and Fabrics, (2013), 132.

[17] D. Bäuerle: "Laser Processing and Chemistry", (Springer-Verlag Berlin Heidelberg, Berlin, Heidelberg, 2011).
[18] J. M. Liu: Opt. Lett., 1981, (1982),
[19] A. Ben-Yakar and R. L. Byer: J. Appl. Phys., 96, (2004), 5316.
[20] C. Park, H. Woon Choi, C. H. Lee, J. J. Lannutti, and D. F. Farson: J. Laser Appl., 26, (2014),
[21] H. W. Choi, J. K. Johnson, J. Nam, D. F. Farson, and J. Lannutti: J. Laser Appl., 19, (2007), 225.
[22] U. Engelhardt, J. Hildenhagen, and K. Dickmann: Laser Tec. J., 8, (2011), 32.
[23] M. Gedvilas and G. Raiukaitis: Proc. SPIE Vol. 6157, (2006),
[24] J. Bonse, S. Baudach, J. Krüger, W. Kautek, and M. Lenzner: Appl Phys A, 74, (2002), 19.
[25] M. Götze, O. Krimig, T. Kürbitz, S. Henning, A. Heilmann, and G. Hillrichs: Phys. Proc., 83, (2016), 147.
[26] S. Preuss, A. Demchuk, and M. Stuke: Appl. Phys. A: Mater. Sci. Process., (1995), 33.
[27] K. Piglmayer, E. Arenholz, C. Ortwein, N. Arnold, and D. Bäuerle: Appl. Phys. Lett., 73, (1998), 847.
[28] G. H. Pettit and R. Sauerbrey: Appl. Phys. A, 56, (1993), 51.
[29] J. Tengsuthiwat, S. Siengchin, R. Berényi, and J. Karger-Kocsis: J. Therm. Anal. Calorim., 132, (2018), 955.
[30] S. T. Hsu, H. Tan, and Y. L. Yao: Polym. Degrad. Stab., 97, (2012), 88.

(Received: June 24, 2018, Accepted: February 17, 2019)